



## Penetration characteristics of the interplanetary electric field to the daytime equatorial ionosphere

C. Manoj,<sup>1,2,3</sup> S. Maus,<sup>1,2</sup> H. Lühr,<sup>4</sup> and P. Alken<sup>1,2</sup>

Received 8 May 2008; revised 25 July 2008; accepted 9 September 2008; published 23 December 2008.

[1] Using 8 years of ionospheric drift measurements from the low-latitude JULIA (Jicamarca Unattended Long-term Investigations of the Ionosphere and Atmosphere) radar and the solar wind and interplanetary magnetic field data from the ACE (Advance Composition Explorer) satellite, we study the characteristics of the prompt penetration of electric fields to the equatorial ionosphere. A large database allowed us to bring out statistically significant characteristics of electric field penetration as a function of frequency. The coherence between the interplanetary electric field (IEF) and the equatorial electric field (EEF) peaks around a 2-hour period with a maximum magnitude squared coherence of 0.6. The coherence is slightly higher (0.7) on magnetically active ( $A_p > 20$ ) days. The cross-phase spectra between the ACE and JULIA variations, after elimination of the propagation delay, have negligible values. Correspondingly, the time shift between IEF and EEF is less than 5 minutes at all periods. We also find that the penetration efficiency is highest during local noon, as compared with that of morning and evening hours. The coherence is lower for days with high solar flux values. We find that the penetration of electric fields into the equatorial ionosphere has no significant dependence on season and on the polarity of IMF  $B_z$ . We propose a transfer function between IEF and EEF, which was validated on synthetic as well as observed IEF data. The use of this transfer function decreases the misfit of a climatological model with the measured equatorial electric field by 27%.

**Citation:** Manoj, C., S. Maus, H. Lühr, and P. Alken (2008), Penetration characteristics of the interplanetary electric field to the daytime equatorial ionosphere, *J. Geophys. Res.*, 113, A12310, doi:10.1029/2008JA013381.

### 1. Introduction

[2] The equatorial day-time ionospheric electric fields exhibit large day-to-day variability. A part of this can be explained in terms of wind-forced, diurnal variations which depend on the location, season, solar irradiation and local time [Scherliess and Fejer, 1999]. Another part of the electric field variation is due to the influence of the interplanetary electric field variations. Abrupt changes as well as quasi-periodic fluctuations of the solar-wind interplanetary electric field (IEF) are known to correlate with the equatorial ionospheric electric field variations. They are called penetrating electric fields [Kelley *et al.*, 1979; Kikuchi *et al.*, 1996; Huang *et al.*, 2005; Nicolls *et al.*, 2007]. In this category, there are two types 1) prompt penetration, and 2) disturbance dynamo effects. Prompt penetration is the immediate response (in a matter of a few minutes) of the ionospheric electric fields to a variation of IEF. The period range of the prompt penetration electric fields in the equatorial ionosphere is a subject of active research [Huang *et al.*, 2007; Fejer *et al.*,

2007]. Various maximum periods have been given, starting from 20 minutes to several hours. The high-velocity meridional neutral winds, set-up by Joule heating of the thermosphere in the auroral region travel to the equatorial region and cause the disturbance dynamo electric field. With a speed of about 600 m/s, these disturbances reach low-latitudes about 4–5 hours after the onset of a storm [Fuller-Rowell *et al.*, 1997]. It has been reported that the effect of disturbance dynamo can persist for more than a day [Scherliess and Fejer, 1997]. The present paper deals with the prompt penetration effects to equatorial ionosphere.

[3] The penetration of the interplanetary electric field (IEF) to the mid and low-latitude ionosphere was first identified by Nishida [1968]. He found that the fluctuations (DP2) observed in ground observatory data were coherent with the interplanetary magnetic field data. The prompt penetration effect was believed to last only up to ~60 minutes because of a shielding effect by the ring current system. For example, the empirical model for the prompt penetration by Fejer and Scherliess [1997] suggested that the effect vanish after 60 minutes. However, Earle and Kelley [1987] argue that the shielding effect by the ring current system is effective only for periods greater than 10 hours. The system, according to them, can act like a capacitor, which allows fluctuations with periods lower than 10 hours to pass through.

[4] Dependence of the prompt penetration on local time, solar flux levels or season has so far not been studied using

<sup>1</sup>CIRES, University of Colorado, Boulder, Colorado, USA.

<sup>2</sup>NGDC NOAA, Boulder, Colorado, USA.

<sup>3</sup>National Geophysical Research Institute, Hyderabad, India.

<sup>4</sup>GeoForschungsZentrum-Potsdam, Potsdam, Germany.

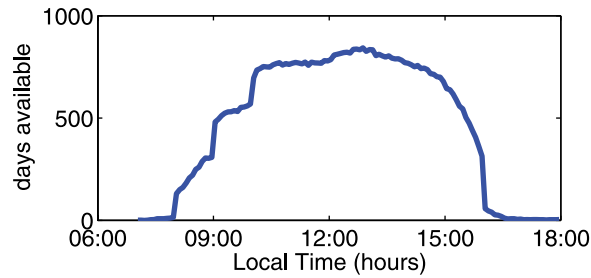


**Figure 1.** Number of available drift measurements versus the local time of JULIA radar.

a sufficiently large database. It is believed that a negative (southward) value for the vertical component of interplanetary magnetic field (IMF),  $B_z$  results in an efficient penetration of the electric fields, because of reconnection between the geomagnetic field and interplanetary magnetic field. However, there are several reports showing prompt penetration while IMF  $B_z$  is northward. It would be interesting to see whether the efficiency of prompt penetration has a dependency on IMF  $B_z$  polarity. Several approaches were made to predict the equatorial ionospheric electric field from proxies of the energy inputs to earth's magnetosphere [e.g., *Huba et al.*, 2005; *Nicolls et al.*, 2007]. However, *Fejer et al.* [2007] comment that the penetration effect is far more complex and cannot be explained by scaling factors or time rates of changes.

[5] One of the difficulties in studying the effect of prompt penetration is to separate it from the effects of the disturbance dynamo. For example, multiple events of IEF fluctuations can result in overlapped effects of prompt penetration and disturbance dynamo in the EEF. Because of the sporadic nature of radar-based ionospheric electric field and/or magnetic field measurements, most of the previous studies were event based. Hence the dependence of the penetration on season, solar-flux, geomagnetic activity and local time were not clear. Also the frequency dependence of electric field penetration to low latitudes is not clearly understood. The JULIA (Jicamarca Unattended Long-term Investigations of the Ionosphere and Atmosphere) measurements offer continuous day-time electric field measurements [*Hysell et al.*, 1997]. Interplanetary electric field data are available from the ACE (Advance Composition Explorer) satellite during this period. This provides an excellent opportunity to derive day-time EEF variations from IEF data. Recently *Huang et al.* [2007] used JULIA drift data and ACE derived IEF to arrive at a linear equation connecting them. Using the ACE-derived IEF data and magnetometer derived EEF data, *Nicolls et al.* [2007] constructed a transfer function to predict EEF variations from IEF. However, both of these studies did not focus the issues we discussed above.

[6] In this paper, we explore the relation of quasi-periodic fluctuations of IEF with that of the equatorial ionospheric electric field. The main objectives of this paper are: (1) to study the coherence and phase difference between IEF and EEF as a function of frequency. We investigate whether the coherence between IEF and EEF is caused by prompt penetration or by a disturbed dynamo effect, (2) to study the dependence of prompt electric field penetration to EEF on season, local time, solar flux, geomagnetic activity and

IMF  $B_z$  polarity, (3) to derive a transfer function to predict day-time ionospheric disturbances from IEF data. We intend to use this transfer function with a climatological model of EEF. Our study doesn't deal with (1) the longitudinal dependency of penetration effects and (2) The effects of penetration in the night-time ionosphere.

[7] We first describe the data sets and processing, followed by the results and discussion.

## 2. Data and Processing

[8] We use the data measured by the ACE satellite and JULIA radar during 1 August 2001 to 8 March 2008 for our study. During this period coincident data were available for 1002 days.

### 2.1. Solar-Wind Electric-Field From ACE

[9] We use the solar wind electric field data from the Advance Composition Explorer (ACE) satellite located at the L1 point (Libration point). The data are obtained from the OMNI Web site. The IEF  $E_y$  component is calculated as  $E_y = -V_x * B_z$ , where  $V_x$  is the solar wind velocity component in the sunward direction and  $B_z$  is the vertical component of the interplanetary magnetic field in Geocentric-Solar-Magnetospheric (GSM) coordinates.  $E_y$  is the dawn-dusk component of the Interplanetary Electric field (IEF). Here, the x-axis points toward the sun, the z axis is perpendicular to the x-axis and is in the plane defined by x-axis and geomagnetic dipole, and the y-axis points toward dusk. The OMNI data sets are primarily intended to support studies of the effects of solar wind variations on the magnetosphere and ionosphere and are time-shifted to the magnetosphere's bow-shock nose from the location of the ACE satellite. For a more detailed description of the processing visit the OMNI Web site (<http://omniweb.gsfc.nasa.gov/>). It has been suggested in the literature to use, for the characterization of the solar wind input, the merging (other names: reconnection, earth-effective) electric field [*Kan and Lee*, 1979],  $E_m = V_x \cdot \sqrt{(B_z^2 + B_y^2)} \cdot \sin^2(\theta/2)$ , where  $B_z$  and  $B_y$  are IMF components and  $\theta$  is the clock angle of the IMF. However, we find that the JULIA drift data has better correlation with  $E_y$  than with  $E_m$ . Hence we use  $E_y$  for our subsequent analysis.

### 2.2. Drift Data From JULIA Radar

[10] The electric field variations of the day-time equatorial ionosphere are derived from JULIA radar measurements. The JULIA radar is located at the Jicamarca radio observatory, Peru (11.95° S geographic latitude, -76.87° E geographic longitude, and ~1° N magnetic latitude). *Hysell et al.* [1997] describe the instrument and first results from JULIA radar. JULIA observes the so called "150-km echoes" and the corresponding vertical Doppler velocity. The data are recorded in 5 min sampling intervals during day time. We use 1002 days of JULIA vertical drift data, during 1 August 2001 to 8 March 2008, for our study. Figure 1 shows the number of JULIA data available as a function of local time. JULIA measures the ionospheric drift during day time from 09–16 LT (13–21 UT).

[11] As we can see, sufficient data are available over the local time sector 08–15 LT. It is necessary to remove the climatological part of the diurnal drift variation to compare

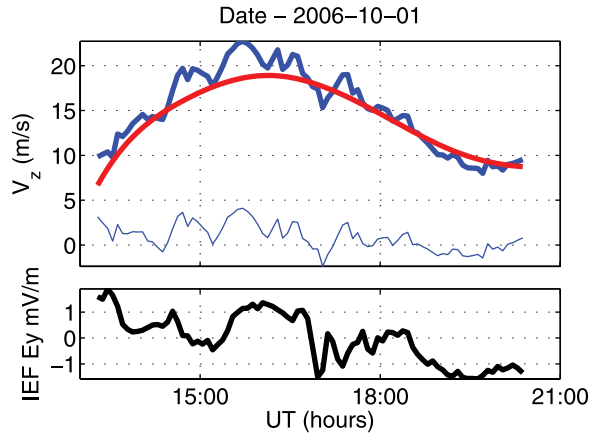


**Figure 2.** An example of the correction of the diurnal variation of the drift data. The observed variation of the drift for 1 October 2006 is presented in blue line. The red line indicates the daily variation, as predicted by the climatological model. (top) Residual drift variation. (bottom) Corresponding IEF data.

the equatorial zonal electric fields with the IEF data. We use a model of the day-time JULIA drift by P. Alken (A quiet-time empirical model of equatorial vertical plasma drift in the Peruvian sector based on 150 km echoes, submitted to *Journal of Geophysical Research*, 2008) to remove the daily drift variations. The model was created from all available JULIA data and is a function of local-time, season, and solar flux. Figure 2 shows an example of daily variation of JULIA drift data and the ACE Ey data (further delayed by 17 minutes) on day 1 October 2006. The vertical drift predicted by the climatological model matches quite well the observed variations. The thin line in Figure 2 (top) shows the residual variations. The IEF Ey, plotted in Figure 2 (bottom) exhibits similar variations.

[12] We calculate the electric field from JULIA drift data by applying the formula  $E_y = -v_z \times B$  [Kelley, 1989, p. 68] where  $v_z$  is the residual vertical drift (observed drift – climatological drift) in m/s and  $B$  is the magnetic field strength obtained from the IGRF model for the Jicamarca site at 150 km altitude. Hereinafter we use the acronyms IEF for inter planetary electric field Ey from ACE satellite and EEF for the residual equatorial zonal electric field derived from the JULIA drift measurements.

### 3. Results

#### 3.1. Coherence

[13] We construct time series pairs of IEF and EEF for the days that satisfy the following criteria. (1) Both EEF and IEF data are available (2) EEF data should be at least six hours long. Though the data were available for 1002 days, the number of days useful for analysis meeting these conditions was 265. The length of individual time series was chosen to be 6 hours. This is a trade-off between long and continuous data interval that we desire and the number of days available for the study. The next step was to estimate the average coherence function between them. Coherence is a function of frequency with values between 0 and 1 that indicate how well one input corresponds to the

output at each frequency. The magnitude-squared coherence is computed as,

$$C_{IEF-EEF}(\omega) = \frac{|P_{IEF-EEF}(\omega)|^2}{P_{IEF-IEF}(\omega) \cdot P_{EEF-EEF}(\omega)}$$

where  $P_{IEF-EEF}$  is the cross-power spectrum between ACE and JULIA and  $P_{IEF-IEF}$  and  $P_{EEF-EEF}$  are their auto spectra. The power spectra and cross spectra are computed by Welch's averaged periodogram method [Welch, 1967]. Fast Fourier transforms (FFT) are performed on each day's JULIA and ACE data multiplied by Hanning window. Periodograms are formed on each window and then periodograms of all windows at each frequency are averaged to yield the power spectra. Cross spectral density is also computed in the same way. We do not overlap the adjacent pairs as they are not contiguous, time-wise (due to the nighttime measurement gaps in JULIA records). The coherence functions is then computed using the average the cross and auto-power spectra. The significance level of coherence was estimated following Thompson [1979]. The significance level is the limit up to which the coherence values can occur by chance. It is given by

$$C_{conf}^2 = 1 - \alpha^{[1/n-1]},$$

where  $\alpha$  is the desired confidence level (here 0.05, equivalent to 95%) and  $n$  is the degrees of freedom (number of days averaged).

[14] We plot the coherence between IEF and EEF in Figure 3. The red line indicates the average over all days. The black line shows the coherence for days with Ap index > 20 (=Kp ~ 3.5). Ap index ranges from 0–400 and is derived from the planetary geomagnetic index, Kp and represents the general geomagnetic activity level. The blue line shows the coherence for days with Ap < 20. The main features of all the coherence functions are the peaks at 2 hours period. The coherence is highest for magnetically active days (0.7), followed by the coherence for all the days (0.6) and for the quiet days (0.5). The coherence

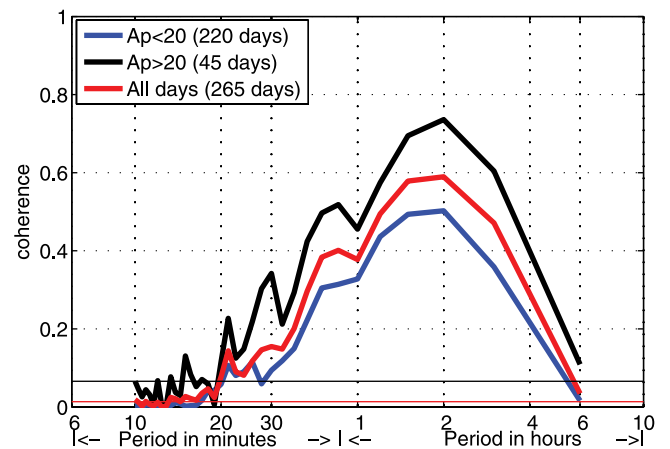


**Figure 3.** The coherence between IEF and EEF. The coherence is higher for days with higher magnetic activity level. The straight lines indicate a significance level of the coherence estimation with 95% confidence interval.

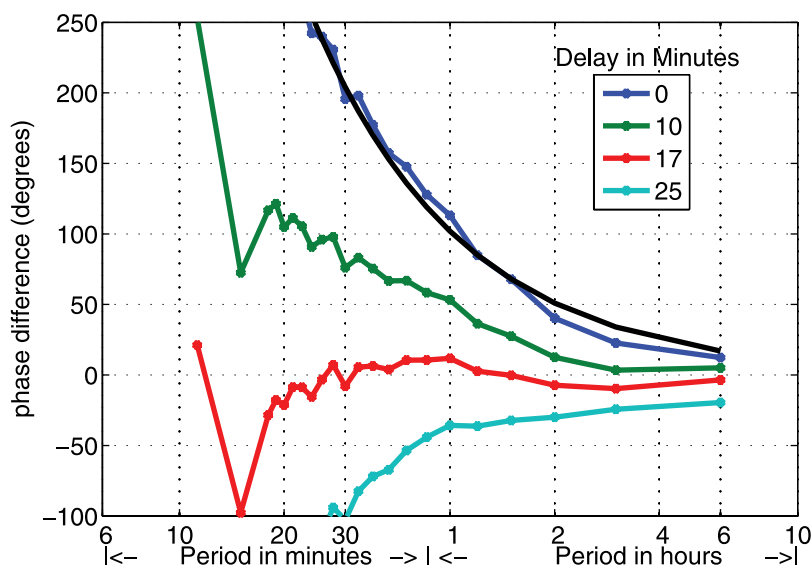


**Figure 4.** Cross phase spectra between IEF and EEF, averaged over all the days considered. The dark blue line shows the phase spectra without time shift correction. Theoretical phase difference corresponding to a 17-minute time delay is plotted with solid black line. The phase spectra for other time delays are also given. It is clear from the figure that a 17-minute delay is most appropriate. The phase spectra are unreliable for periods less than 20 minutes.

spectra appear to have multiple peaks between 20 minutes and 2 hours period. This is more pronounced for days with  $A_p > 20$ . The coherence estimates are statistically significant for periods higher than 20 minutes in all the three conditions.

### 3.2. Phase Difference

[15] We now examine the phase difference between IEF and EEF as a function of frequency. From all the available data, we compute average cross-phase spectra between ACE and JULIA. Before we study the phase spectra, we need to correct a time delay between IEF and EEF data. The correction is for the time taken by the solar wind signals to propagate from the bow shock to the equatorial ionosphere. Note that the time delay for solar wind to propagate from the satellite position (L1 point) to bow-shock is accounted for by the OMNI processing. We plot the cross-phase spectra between IEF and EEF derived from all days in Figure 4. The blue line indicates the phase spectra with unshifted IEF data. The monotonous decrease of phase with increase in period is the effect of a time delay. We plot a predicted phase spectrum ( $2\pi f \cdot \Delta t$ —solid black line) for two time series time-shifted by 17 minutes. The observed phase values matches well with the predicted spectra. We plot the phase spectra with different successive delays. It is clear from Figure 4 that a 17 minutes time delay is the most appropriate time delay for solar wind electric fields to propagate from bow-shock to equatorial ionosphere.

[16] It may be noted that this time-delay is an average over all the days. It is possible that some events (penetration) may have slightly different time delays. Once we delay IEF, the phase spectra have negligible values for all the periods we consider. The residual time delay between IEF and EEF never exceeds 5 minutes. We discuss the implication of

this finding in section 5. In the subsequent analysis, we always delay IEF data by 17 min.

### 3.3. Dependence on Local Time

[17] We examine the local time dependence of the electric field penetration to the day-time equatorial ionosphere. In order to separate the effects of different local times, we select 3-hour long windows centered at LTs 10:30, 11:30, 12:30, 13:30 and 14:30. By limiting our study between late morning and early evening, we do not include the possible influence of the EEF reversals in the morning and evening. The average coherence function is estimated from pairs of IEF and EEF (each with 3 hours length) following the approach we discussed earlier. The coherence function is thus limited to a period range from 10 minutes to 3 hours. Figure 5a shows the coherence plots for different LT ranges. The coherence is highest when we correlate the EEF measured during 10–13 (window is centered at 11:30) to IEF data. The coherence has a peak value of 0.7 at the 2 hours period. EEF data centered at 12:30 (measured during 11–14 LT) and at 1:30 (measured during 12–15 LT) shows comparatively smaller coherence values. Lowest coherence functions between EEF and IEF were obtained when considering EEF data during morning (09–12 LT) and afternoon (13–16 LT). It appears that prompt penetration to the equatorial ionosphere is most efficient during local noon. It is, however, worth noting that the secondary spectral peak at 40 minutes shows almost no local time dependence.

### 3.4. Dependence on IMF Polarity

[18] The IMF variation in N–S direction causes zonal electric field perturbations in the ionosphere through penetration of the IEF. To examine whether there is a difference in the efficiency of electric field penetration during IMF  $B_z$

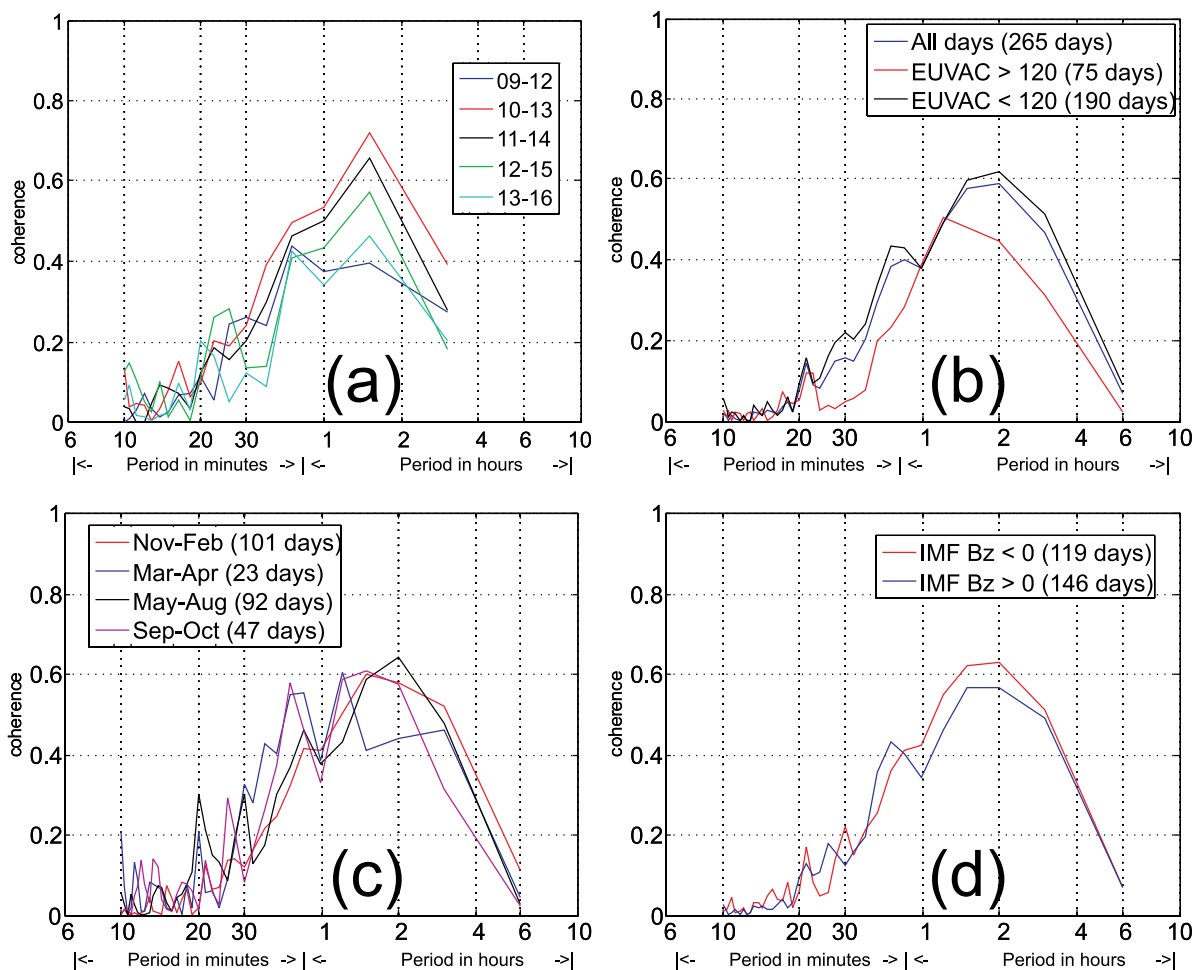


**Figure 5.** Dependence of the coherence between IEF and EEF on (a) local time, (b) solar flux, (c) season, and (d) IMF  $B_z$  condition.

positive and negative phases, we divide our database into two corresponding groups (IMF  $B_z > 0$  and IMF  $B_z < 0$ ). We have 146 days of IMF  $B_z$  positive and 119 days of IMF  $B_z$  negative conditions. Figure 5d shows the coherence plots for these periods between IEF and EEF. We can see that the coherence is almost identical during both conditions, except that negative IMF  $B_z$  conditions result in slightly larger values of coherence at longer periods (1–3 hours).

### 3.5. Dependence on Season and Solar-Flux

[19] The coherence estimation was carried out by grouping the observations into four seasons. November–February (Southern Summer), May–August (Southern Winter), March–April and September–October (equinoxes). Figure 5c shows the coherence plot for the different seasons. The coherence functions for summer and winter are almost identical. The coherence functions during the two equinox periods are slightly different. The equinox coherence show slightly higher values up to a period 40 minutes. However, the differences themselves are not significant enough to warrant further discussion. Our conclusion is that the prompt penetration effects (at least up to 6 hours) are not significantly affected by the season.

[20] The data set used here spans from solar maximum (2001) to solar minimum conditions (2008). We examine,

whether the prompt penetration effect has a dependency on the solar flux level. We plot the coherence functions for different conditions of EUVAC. EUVAC is Extreme Ultraviolet (EUV) flux model for aeronomic calculations which is calculated as  $0.5 * (F_{10.7} + F_{10.7A})$ , where  $F_{10.7A}$  is the 81-day moving average of  $F_{10.7}$  [Richards *et al.*, 1994]. It has been shown that for ionospheric studies, EUVAC is a better proxy of solar irradiance than  $F_{10.7}$ . We plot the coherence between IEF and EEF in Figure 5b. The dependency on EUVAC is clear in Figure 5b. The coherence between IEF and JULIA electric fields is lower for days with EUVAC > 120. The majority of the days used for the analysis fall into solar flux values lower than 120. An obvious explanation is the inverse relation of ionospheric conductivity and prompt penetration as suggested by Fejer *et al.* [2007].

### 4. Transfer Function

[21] We construct a transfer function between the EEF and IEF data using all days for this purpose. The transfer function is the quotient of the cross-power spectral density ( $P_{IEF-EEF}$ ) of the two data sets and the power spectral density of the input ( $P_{IEF-IEF}$ ). In this case the input data set is the IEF and output data set is the EEF. The averaged

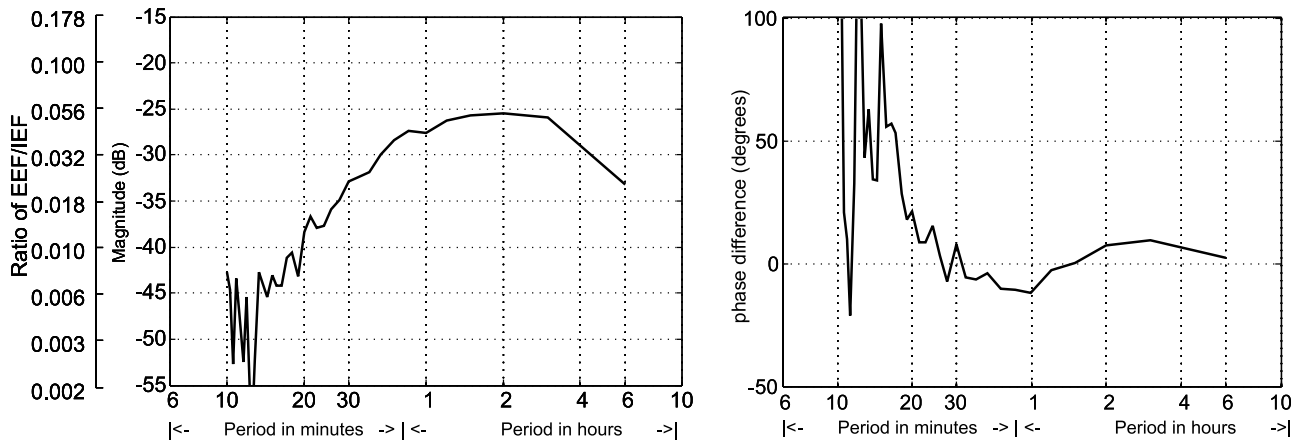


**Figure 6.** Transfer function between IEF and IMF, estimated using all the available days. (left) Magnitude of the transfer function. (right) Phase of the transfer function.

cross and auto-power densities were estimated as described in the previous section. The equation for the transfer function is,

$$T_{IEF-EEF}(\omega) = \frac{P_{EEF-IEF}(\omega)}{P_{IEF-IEF}(\omega)}$$

We plot the magnitude of the transfer function in Figure 6 in a non-dimensional unit, decibel (dB). Decibel is a logarithmic measure of a ratio between input and output signal. It is calculated as  $20 \cdot \log_{10}(|T_{IEF-EEF}|)$ . For example a magnitude of  $-20$  dB indicates an EEF/IEF ratio of 0.1 at that period. Similarly,  $-40$  dB indicate a ratio of 0.01. The main feature of the transfer function is the broad peak around 2 hours, indicating maximum admittance of the IEF to EEF at this period. On both flanks of this peak, the transfer function magnitude decreases. The 2-hour peak of the transfer function magnitude is in agreement with a study carried out by *Nicolls et al.* [2007], using ACE IEF data and magnetometer derived EEF from Jicamarca. A major difference between two transfer functions is the slightly higher magnitude shown by our transfer function, especially toward smaller periods. Between 2 hours and 30 minutes, our transfer function shows a loss of magnitude by 7 dB, as

compared to 15 dB in the result of *Nicolls et al.* [2007]. This is due to the fact that, since JULIA measures the drift directly, more high-frequency information about the electric field variations is captured in our study as compared to the magnetometer-inferred EF data used by them. The drift is directly related to the electric fields in contrast to the magnetometer which is sensitive to the electric currents which are modulated by the conductivity of the ionosphere.

[22] Figure 6 (right) shows the phase of the transfer function. The phase values are negligible for periods greater than 30 minutes, where IEF and EEF are significantly coherent. Hence the transfer function does not induce relative time delays among the considered frequency range.

**4.1. Application to Synthetic Data**

[23] We test the transfer function derived between IEF and EEF data with a set of synthetic time series of IEF as input. Previously, *Senior and Blanc* [1984], *Spiro et al.* [1988], *Fejer et al.* [1990] and *Huba et al.* [2005] used a step function of Auroral Electrojet (AE) index/Polar cap potential as an input to their model to examine the effect on the equatorial ionosphere. Recently, *Huang et al.* [2007] and *Nicolls et al.* [2007] described the use of synthetic step and triangle functions to examine the response of the equatorial

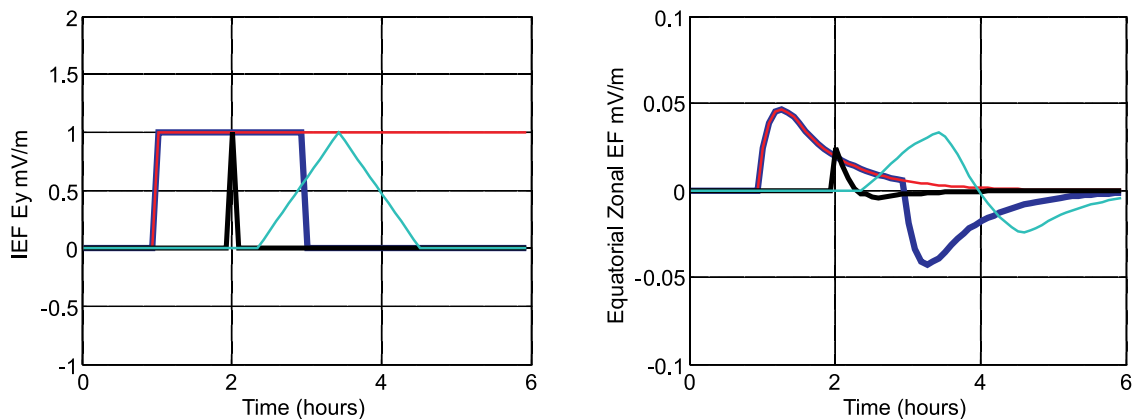


**Figure 7.** (left) Synthetic time series of IEF and (right) responses of the transfer function, when applied to the synthetic time series.

ionosphere. Uses of these synthetic functions can provide interesting insight into the behavior of the system. As we will see in the application sections, IEF shows abrupt changes on many occasions resembling step and spike functions, at least within the time resolution considered.

[24] Figure 7 (left) shows the synthetic IEF time series. The red line shows a step function. The box function (blue line) and the triangle function (cyan line) are both 2 hours in duration. The spike function is represented by a black line. Peak amplitudes of all the functions are 1 mV/m. The responses of the average transfer function to these input time series are shown in Figure 7 (right). The step function produces a sudden positive response in EEF data peaking at an amplitude of 0.045 mV/m. This is followed by a slow decay of the signal. The immediate response of a box function is the same as that of a step function. The decay phase is disturbed by the reversal of the input function. The triangle function is slower in build up of energy and hence its response in EEF is different from box and step functions.

#### 4.2. Application to Measured IEF Data

[25] We apply the average transfer function to 8 days of ACE IEF data and compare the response with the JULIA-inferred EEF data. We chose the days so as to include broadly different seasons and geomagnetic activity levels. In Figures 8a to 8h we plot the observed and predicted EEF along with the ACE IEF data.

##### 4.2.1. Figure 8a: 17 August 2001, Mean $A_p = 132.0$ (Southern Winter)

[26] The IEF shows a variation of  $\pm 10$  mV/m during this geomagnetically active day. The observed EEF shows variations within  $\pm 0.4$  mV/m. The transfer function based prediction follows the major features of the EEF variations. Especially, the spike-like variation of IEF causes a major reduction in the EEF, which is reproduced exactly by the transfer function (21:30 UT). However, the positive excursion of the observed EEF, just before this event, is not predicted by the transfer function, since there was no causative variation in the IEF data.

[27] Figure 8b: 2 October 2001,  $A_p = 80.0$  (Equinox). The IEF displays a sharp step like variation starting at UT 15:00. The IEF remains in this positive phase at least for the next 9 hours. The response of the EEF to this signal is similar to the one we discussed in the synthetic test. The sudden positive offshoot is followed by a gradual decay of the EEF. The transfer-function based prediction of the EEF closely follows the observed response. However the observed and predicted EEF differ after 17 UT, most probably due to unreliable drift data. The DC shift between the predicted and observed EEF is probably due to an underestimation of climatological variations.

[28] Figure 8c: 5 April 2003,  $A_p 47.5$  (Equinox). The IEF variations repeat a box-like function, starting at 17 UT and 19UT each lasting for about two hours. These fluctuations are manifested in the observed EEF as similar shaped variations. The predicted signals (shown in blue color) closely follow the observations. Especially the offshoot (sharp jump of the predicted/observed signal at the beginning of a box-function) and decay are reproduced.

[29] Figure 8d: 21 June 2003,  $A_p = 19.5$  (Southern Winter). During this moderately quiet day, we see a sudden

decrease in the IEF near 17 UT. This produces the expected response in the EEF and it is reproduced by the transfer function output. However, the transfer function predicts a faster recovery of the EEF between 18 UT and 20 UT than is shown by the observed EEF. The fluctuations around 15 UT are also well reproduced by the transfer function.

##### 4.2.2. 30 October 2004 (Equinox-Figure 8e) and 22 January 2006 (Southern Summer-Figure 8f)

[30] These days have low  $A_p$  values. The fluctuations in the observed EEF are closely predicted by the transfer function.

[31] Figure 8g: 2 September 2005,  $A_p 89.0$  (Equinox). This was a relatively active day during Equinox. The IEF shows a series of fluctuations, starting at 15 UT. The corresponding responses of the observed EEF are broadly predicted by the transfer function. However, the transfer function output underestimates the observed peak amplitudes at 15, 16:30 and 19 UTs.

[32] Figure 8h: 12 January 2008,  $A_p = 15$  (Southern summer). The last plot shows an IEF variation similar to a box function, starting at 15 UT. The IEF was positive from 15 UT to 17 UT. During this time, the observed EEF showed an initial offshoot followed by slow decay of the signal until 17:30 UT, when IEF reversed its polarity to negative values. The predicted EEF closely follows the initial response, however, it decays faster than the observed data.

## 5. Discussion and Conclusion

[33] We described the relation between the Interplanetary Electric Field (IEF) and the Equatorial ionospheric zonal Electric Field (EEF) at Jicamarca using eight years of data. We computed the coherence between IEF and EEF for periods up to 6 hours and examined its dependency on season, local time, solar flux and IMF  $B_z$  conditions. In this section, we discuss implications of our results.

[34] Frequency dependency of the electric field prompt penetration was reported in an earlier work by *Earle and Kelley* [1987]. They compared radar-based electric field measurements between a high-latitude and a low-latitude region. They found that for the period range 1–10 hours the penetration effects dominate the climatological effects in the low-latitude ionosphere during magnetically active periods ( $K_p > 3$ ). They obtained highest efficiency of penetration for periods 3–5 hours. We find that the coherence between IEF and EEF is highest for periods around 2 hours during days with  $A_p > 20$ , as compared to those with  $A_p < 20$ . However, even during magnetically quiet days the coherence is significant. This doesn't imply that the penetration signals dominate the atmospheric/climatological variation during quiet days. However, the prompt penetration signal at Jicamarca has sufficient power to be measured by the radar even during quiet periods. *Abdu et al.* [2003] showed evidence for prompt penetration even on an extremely quiet day. The peak coherence around 2 hours between IEF and EEF is in agreement with the broad peak of the transfer function between IEF and EEF proposed by *Nicolls et al.* [2007]. The peak in coherence indicates that the system that couples magnetosphere and the equatorial ionosphere has a preferred response in the period range around 2 hours.

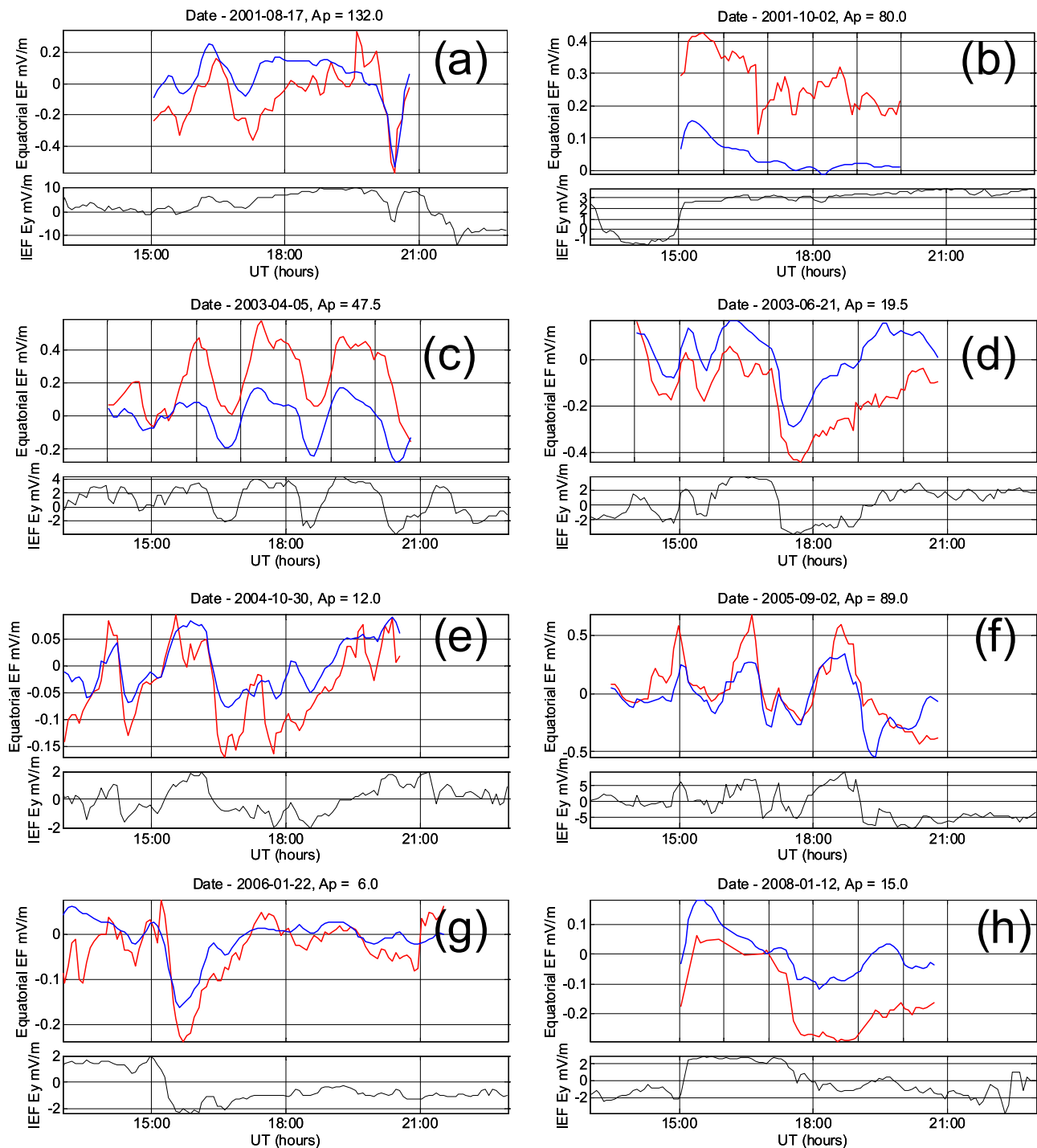


**Figure 8.** Application of the average transfer function on ACE IEF data. The red line indicates the observed EEF inferred from JULIA, and the blue line indicates the predicted EEF. The lower rows show the corresponding IEF data.

[35] This is the first time that cross-phase spectra between IEF and JULIA measured EEF are reported. A large database allowed us to look into the phase spectra between the two data sets. Our aim was to find out whether their cross-phase spectra are frequency-dependent. We find that the time delay between the IEF and the EEF is less than 5 minutes for all harmonics in the period range considered

here. Since there is no frequency-dependent phase delay associated with IEF and EEF, we can conclude that the process that causes the coherence between the two signals in our study is consistent with the prompt penetration. This is in contrast to the comments by *Fejer* [2002] suggesting that the prompt penetration effect essentially vanishes after 1 hour. It is possible that the EEF data we used are also



affected by electric fields due to disturbance dynamo action. However, in the average cross-spectral estimates presented here, the effect of disturbance dynamo will be averaged out. This is due to the fact that while PP is fast and its effect is immediate at equatorial latitudes, the onset time of the disturbance dynamo effect in the equatorial region varies from event to event. In addition, as pointed out by *Maruyama et al.* [2005], the disturbance dynamo dominates over prompt penetration only in the evening hours, whereas our analysis is limited to local day-time.

[36] We also give evidence that the prompt penetration doesn't cause relative phase variation greater than 5 minutes between different harmonics of IEF and EEF. *Kobeia et al.* [2000] compared magnetic data during a geomagnetic storm from a high-latitude and a low-latitude station and found them highly coherent within periods 25–75 min. More importantly, they could not find any phase differences between the high-latitude and equatorial data sets. Other than the constant time delay caused by the propagation of solar wind signals from the L1 point to the auroral regions, we do not find any phase difference between the two data sets. There is wide consensus that prompt propagation of electric fields from high to low latitude is very fast (<1 min). Our finding is that the transition from solar wind to high latitude is frequency-independent. We find that the optimum propagation time of the IEF from the magnetosphere's bow-shock nose to the equatorial ionosphere is 17 minutes. The propagation time can be broken down into three parts: The solar wind takes 3–4 minutes to travel from the bow shock nose to the magnetopause: a distance of about 3 Re and with a speed of 100 km/s. The remaining 14 minutes are due to the propagation from magnetopause to high-latitude ionosphere [e.g., *Vennerström et al.*, 2002]. The prompt penetration is very fast between high- and low-latitude ionosphere [e.g., *Kobeia et al.*, 2000].

[37] The most obvious local time effect of prompt penetration to the equatorial ionosphere is the difference between day and night. The IEF variation that causes penetrating eastward electric fields on the day-side equatorial ionosphere will cause a westward electric field in the night-side ionosphere [e.g., *Fejer*, 2002]. Our interest is to study the local-time dependence of prompt penetration to the day-time equatorial ionosphere. During the JULIA measurement period (08–16LT), the ionospheric conductivity undergoes variations due to EUV ionization and  $E \times B$  related plasma uplift. The conductivity reaches a maximum during local noon time. It is believed that in the mid and low-latitude ionosphere, the penetration electric field is inversely proportional to the ionospheric conductivity [e.g., *Fejer*, 2002]. However, we see that the coherence between IEF and EEF is maximal when we use a 3-hour long window centered on local noon-time. The morning and afternoon hours show lower coherence between IEF and EEF, at least for the long-period variations. Many of the previous studies have looked at events away from noon when the 0.7 hours (~40 minutes) peak becomes more prominent. Since the polar potential difference is maximal between dawn and dusk, we speculate that the prompt penetration effect is maximally aligned east–west during local noon time and weaker during morning and evening. Hence the radar measurements at an equatorial station will be most sensitive to prompt penetration during local noon. In addition, as pointed out

by *Chau and Kudeki* [2006], the “150 km echoes” from the ionosphere, which are used in the JULIA radar measurements to determine the EEF, become less frequent and have lower power before 9:00 LT and after 15:00 LT.

[38] *Fejer and Scherliess* [1997, Figure 5] showed the response of the equatorial ionospheric drift to a step function in the polar cap potential (PCP). They found that the effect on the drift vanish 60 minutes after the start of the step function. *Huba et al.* [2005] presented a simulation using a fully coupled, self-consistent model of the inner magnetosphere and global ionosphere. *Huang et al.* [2007] applies this model to a step and a triangle function of PCP and find that the EEF vanish within 60 minutes of the perturbations in the PCP. In contrast, the transfer function we presented shows longer (up to 3 hours) effect on the equatorial electric field to a step function of IEF. Note that above models produce equatorial responses only on the increase (under shielding effects) of the PCP, whereas our transfer function includes both increasing and decreasing cases of IEF. Our results are more comparable with the characteristics of the transfer function between IEF and EEF presented by *Nicolls et al.* [2007]. They use IEF and magnetometer derived EEF to produce a transfer function between them. The amplitude of the immediate response of EEF (offshoot) to IEF perturbations, predicted by our transfer function is slightly higher (0.045 mV/m) than that by *Nicolls et al.* [2007]. The immediate response of our transfer function is superior to that of *Nicolls et al.* [2007] since the JULIA-derived EEF has higher frequency resolution than the magnetometer derived EEF. *Nicolls et al.* [2007] show that the response (prompt penetration) of the equatorial ionosphere due to a step function in IEF lasts for more than 6 hours. However, the response of our transfer function is negligible after 3 hours. It is possible that the long-period response shown by *Nicolls et al.* [2007] is due to the lack of a background model that dampens their quasi-DC responses. It may be noted that the 6-hour limitation of the time length of the data pairs considered here makes the long period (>3 hours) response of our transfer function less certain. There are some indications in Figure 8 that our transfer function underestimates the long periods. Finally, it should be noted that our transfer function is an average over all magnetospheric/ionospheric conditions. Hence the transfer function may not explain all the prompt-penetration effects on EEF.

[39] Another objective of our paper is to study the use of the transfer function to add day-to-day variability to a climatological model. We compute the daily variation of EEF by subtracting the EEF given by a climatological model of the JULIA drift data (Alken, submitted manuscript, 2008). This has been done for 663 days from 2001–2008. The root mean square (RMS) of the daily variation of EEF (averaged over all the days) was 0.0537 mV/m. We then predict the daily variation by applying the transfer function with ACE derived IEF as input. The transfer function could explain 27% of this daily RMS. On magnetically active days (defined as  $A_p > 20$ ), the RMS of daily variation was 0.1369 mV/m, of which 38% was due to prompt-penetrating electric fields. The results are summarized in Table 1.

[40] This shows that we can explain around 27% of the residuals, which are obtained when subtracting a climato-

**Table 1.** Average Daily RMS Values of Residual EEF From 663 Days<sup>a</sup>

Description	RMS of Daily Variation (Observation, Climatological Model) [mV/m]	Residuals Explained by Penetration	
		mV/m	%
All days (663 d)	0.0537	0.0146	27.2
Ap > 20 (145 d)	0.1369	0.0521	38.0

<sup>a</sup>Daily EEF variations derived from the climatological model are subtracted from the observed EEF to obtain the residuals. The transfer function is then made to predict the EEF from the IEF data.

logical model from the actual EEF measurements, by predicting the penetration effects with the help of our transfer function.

## 6. Summary and Conclusions

[41] We studied the relationship between the interplanetary electric fields (IEF) and the equatorial ionospheric electric field (EEF) as a function of frequency. We used eight years of IEF data from the ACE satellite and equatorial ionospheric drift data from the JULIA radar. We limited our study to local day-time at the JULIA location and period from 10 minutes to 6 hours. We computed the coherence between the two data sets and examined its dependency on geomagnetic activity level, local time, season, solar flux and IMF  $B_z$  conditions. We also constructed a transfer function between IEF and EEF and compared the predicted data with the observed data. Further, we examined the use of the transfer function to reduce the variance of a climatological model for JULIA drift. Our findings are summarized as:

[42] 1. The coherence between IEF and EEF peaks around 2 hours period with a maximum magnitude squared coherence of 0.6. We find that the coherence is higher (0.7) during magnetically active days (defined here as Ap > 20).

[43] 2. Optimum propagation time for the IEF to travel from the magnetosphere's bow-shock nose to the equatorial ionosphere is 17 minutes. The phase difference between the IEF and EEF (after delaying IEF with optimum delay time) is within  $\pm 13^\circ$  for the entire period during which the two data set are coherent. The lack of relative phase differences in their frequency range indicates that, the process that makes the IEF and EEF signals coherent is consistent with the prompt penetration. In addition, there seems to be no phase modulation of the interplanetary signal while it propagates through the magnetosphere.

[44] 3. We examine the dependence of electric field penetration on the local time at JULIA station. We find that the coherence is around 0.7 when using only data around noon-time, as compared to relatively lower coherencies for morning and evening hours.

[45] 4. The coherence between IEF and EEF is lower for days with high solar flux levels (defined as EUVAC > 120) as compared to days with lower solar flux levels. We find that the prompt penetration of electric fields into the equatorial ionosphere has no significant dependence on season and on the polarity of IMF  $B_z$ .

[46] 5. We estimated a transfer function between IEF and EEF, which was validated on synthetic as well as observed IEF data. We find that the use of this transfer function

decreases the misfit between predicted and observed equatorial electric fields by an average of 27%, over using a purely climatological model.

[47] **Acknowledgment.** Wolfgang Baumjohann thanks the reviewers for their assistance in evaluating this paper.

## References

- Abdu, M. A., C. M. Dinardini, J. H. A. Sobral, I. S. Batista, P. Muralikrishna, K. N. Iyer, O. Veliz, and E. R. de Paula (2003), Equatorial electrojet 3-M irregularity dynamics during magnetic disturbances over Brazil: Results from the new VHF radar at Sao Luis, *J. Atmos. Terr. Phys.*, *65*(14–15), 1293–1308.
- Chau, J. L., and E. Kudeki (2006), First E- and D-region incoherent scatter spectra observed over Jicamarca, *Ann. Geophys.*, *24*(5), 1295–1303.
- Earle, G. D., and M. C. Kelley (1987), Spectral studies of the sources of ionospheric electric fields, *J. Geophys. Res.*, *92*(A1), 213–224.
- Fejer, B. G. (2002), Low latitude storm time ionospheric electrodynamics, *J. Atmos. Terr. Phys.*, *64*(12–14), 1401–1408.
- Fejer, B. G., and L. Scherliess (1997), Empirical models of storm time equatorial zonal electric fields, *J. Geophys. Res.*, *102*(A11), 24,047–24,056.
- Fejer, B. G., et al. (1990), Low- and mid-latitude ionospheric electric fields during the January 1984 GISMOS campaign, *J. Geophys. Res.*, *95*(A3), 2367–2378.
- Fejer, B. G., J. W. Jensen, T. Kikuchi, M. A. Abdu, and J. L. Chau (2007), Equatorial ionospheric electric fields during the November 2004 magnetic storm, *J. Geophys. Res.*, *112*, A10304, doi:10.1029/2007JA012376.
- Fuller-Rowell, T. J., M. V. Codrescu, R. G. Roble, and A. D. Richmond (1997), How does the thermosphere and ionosphere react to a geomagnetic storm?, in *Magnetic Storms*, *Geophys. Mon. Ser.*, vol. 36, edited by B. T. Tsurutani et al., pp. 203–225, AGU, Washington, D. C.
- Huang, C.-S., J. C. Foster, and M. C. Kelley (2005), Long-duration penetration of the interplanetary electric field to the low-latitude ionosphere during the main phase of magnetic storms, *J. Geophys. Res.*, *110*, A11309, doi:10.1029/2005JA011202.
- Huang, C.-S., S. Sazykin, J. L. Chau, N. Maruyama, and M. C. Kelley (2007), Penetration electric fields: Efficiency and characteristic time scale, *J. Atmos. Terr. Phys.*, *69*(10–11), 1135–1146.
- Huba, J. D., G. Joyce, S. Sazykin, R. Wolf, and R. Spiro (2005), Simulation study of penetration electric field effects on the low- to mid-latitude ionosphere, *Geophys. Res. Lett.*, *32*, L23101, doi:10.1029/2005GL024162.
- Hysell, D. L., M. F. Larsen, and R. F. Woodman (1997), JULIA radar studies of electric fields in the equatorial electrojet, *Geophys. Res. Lett.*, *24*(13), 1687–1690.
- Kan, J. R., and L. Lee (1979), Energy coupling function and solar wind-magnetosphere dynamo, *Geophys. Res. Lett.*, *6*(7), 577–580.
- Kelley, M. C. (1989), *The Earth's Ionosphere: Plasma Physics and Electrodynamics*, Academic Press, San Diego, Calif.
- Kelley, M. C., B. G. Fejer, and C. A. Gonzales (1979), An explanation for anomalous equatorial ionospheric electric fields associated with a northward turning of the interplanetary magnetic field, *Geophys. Res. Lett.*, *6*(4), 301–304.
- Kikuchi, T., H. Lühr, T. Kitamura, O. Saka, and K. Schlegel (1996), Direct penetration of the polar electric field to the equator during a DP 2 event as detected by the auroral and equatorial magnetometer chains and the EISCAT radar, *J. Geophys. Res.*, *101*(A8), 17,161–17,173.
- Kobe, A. T., A. D. Richmond, B. A. Emery, C. Peymirat, H. Lühr, T. Moretto, M. Hairston, and C. Amory-Mazaudier (2000), Electrodynamic coupling of high and low latitudes: Observations on May 27, 1993, *J. Geophys. Res.*, *105*(A10), 22,979–22,989.
- Maruyama, N., A. D. Richmond, T. J. Fuller-Rowell, M. V. Codrescu, S. Sazykin, F. R. Toffoletto, R. W. Spiro, and G. H. Millward (2005), Interaction between direct penetration and disturbance dynamo electric fields in the storm-time equatorial ionosphere, *Geophys. Res. Lett.*, *32*, L17105, doi:10.1029/2005GL023763.
- Nicolls, M. J., M. C. Kelley, J. L. Chau, O. Veliz, D. Anderson, and A. Anghel (2007), The spectral properties of low latitude daytime electric fields inferred from magnetometer observations, *J. Atmos. Terr. Phys.*, *69*(10–11), 1160–1173.
- Nishida, A. (1968), Coherence of geomagnetic DP 2 fluctuations with interplanetary magnetic variations, *J. Geophys. Res.*, *73*(17), 5549–5559.
- Richards, P. G., J. A. Fennelly, and D. G. Torr (1994), EUVAC: A solar EUV flux model for aeronomic calculations, *J. Geophys. Res.*, *99*(5), 8981–8992.
- Scherliess, L., and B. G. Fejer (1997), Storm time dependence of equatorial disturbance dynamo zonal electric fields, *J. Geophys. Res.*, *102*(A11), 24,037–24,046.

- Scherliess, L., and B. G. Fejer (1999), Radar and satellite global equatorial  $F$  region vertical drift model, *J. Geophys. Res.*, *104*(A4), 6829–6842.
- Senior, C., and M. Blanc (1984), On the control of magnetospheric convection by the spatial distribution of ionospheric conductivities, *J. Geophys. Res.*, *89*(A1), 261–284.
- Spiro, R. W., R. A. Wolf, and B. G. Fejer (1988), Penetration of high-latitude electric fields effects to low latitudes during SUNDIAL 1984, *Ann. Geophys.*, *6*, 39.
- Thompson, R. O. (1979), Coherence significance levels, *J. Atmos. Sci.*, *36*, 2020–2021.
- Vennerstrøm, S., T. Moretto, N. Olsen, E. Friis-Christensen, A. M. Stampe, and J. F. Watermann (2002), Field-aligned currents in the dayside cusp and polar cap region during northward IMF, *J. Geophys. Res.*, *107*(A8), 1188, doi:10.1029/2001JA009162.
- Welch, P. (1967), The use of fast Fourier transform for the estimation of power spectra: A method based on time averaging over short, modified periodograms, *IEEE Trans. Audio Electroacoust.*, *15*(2), 70–73.
- 
- P. Alken, C. Manoj, and S. Maus, CIRES, University of Colorado, 325 Broadway, Boulder, CO 80305-3328, USA. (manoj.c.nair@noaa.gov)  
H. Lühr, GeoForschungsZentrum-Potsdam, Telegrafenberg, 14473 Potsdam, Germany.